Unique Aspects of the Design and Construction of the Bristol Motor Speedway CRC Pavement

Stephen Swift[1], D. Zollinger, P.E., Member ISCP[2], A.Bhasin[3], E. Masad, P.E.[4], Anol Mukhopadhyay[5]

Abstract

The reconstruction of the Bristol Motor Speedway (BMS) track surface presented some unique challenges to the placement of a continuously reinforced concrete (CRC) pavement. Due to the steep embankments of the radial sections, it was not feasible to use a traditional type of bond breaker to isolate the CRC from the subbase layer and so it was determined to bond the CRC to the base and eliminate the interlayer from the pavement section. Reflection cracking from the subbase was a concern and as a counter measure special crack control precautions were taken to insure the uniformity of the crack pattern using early aged crack control which required additional modifications to the sawing equipment to adopt it to the geometry of the track. The design of the steel was also configured to account for the bonded condition and the geometry of the track.

Introduction

Figure 1 BMS with 160,000 fans.

In the fall of 2006, the Bristol Motor Speedway (Figure 1), the site of the 'Sharpie 500' which is one of the sponsored, bi-annual NASCAR track events, determined the main track area should be removed and replaced in order to improve track safety, functionality, and longevity. This track features two banked curves to an exceptional 30 degrees which makes this the fastest half-mile (0.53 mile to be exact) track on the NASCAR circuit. The speedway is located in the extreme northeast corner of the state, near the West Virginia, North Carolina and Virginia state lines. Speedway Motorsport Inc., owners of the track, decided to totally remove the existing post-tensioned concrete track and replace it with a new continuously reinforced concrete (CRC) pavement. The original track, constructed in 1992, consisted of a 4 inch post-tensioned slab (with cables running at 12" O.C. in the longitudinal direction and 3' O.C. in the transverse direction) that was designed into 4 sections via expansion joints at the quarter points of the oval track to serve as points of stress relief. Over the years due to poor drainage and modifications to the original design, the post tensioned concrete had been subjected to considerable deterioration and cracking that in part appeared to be alkali-silica reactivity (ASR) related, creating weakened sections in and around cable anchor points (Figure 2). These weakened areas in the track were becoming a source of constant maintenance and threatened the operational functionality of the track.

Investigation of Track Deterioration

The track was designed with 4 expansion joints or termination points for tensioning and stress relief purposes. These areas created 4 different slabs (one in each full turn and then the 2 straight a ways). The post-tensioned slab only provided 14 years of service as it had under gone a series of worsening consequences mainly at the expansion joints due to thermal expansion and contraction in the track. Early in the life of the pavement, restriction induced at the joints essentially caused the track to constantly move inward. As the slab, particularly through the turns would contract, it would creep down the slope towards the infield of the track. Temperature induced expansion within the oval track could not overcome the force of gravity causing failure at the expansion joints (Figure 3) in the post-tensioned track. 2" of concrete were cut out of the track on the night before the race in March 2007. The joints had moved from 2" to 0" in a matter of 3 weeks of warm weather.

Figure 2 Failed cable anchor.

Visual inspection of the existing track concrete suggested the cause of the deterioration was ASR related based on the characteristic 'Y' shaped cracking present at the surface of the pavement. With this in mind, the analyses were initially aimed at identifying ASR evidence. Subsequent investigation indicated the distress could also be attributed to sulfate attack or even simple freeze-thaw cycles. To this end, several tests to validate any of these suspicions were performed. Analysis consisted of visual and petrographic examination, accelerated aggregate reactivity testing, X-ray diffraction, and assessment of sulfate ion concentration of the soil ground water from the site.

Figure 3 Expansion Joint Failure.

Petrographic Examination

Three - four inch diameter cores were obtained from the existing concrete track. Visual analysis of the cores indicated severe cracking and weathering to depths of 2-3 inches from the surface. This weathering of this nature seems to suggest that the cracking occurred early and allowed air and water penetration over an extended period of time. Thin section slides of the cores yielded the following observations:

1. Occurrences of ettringite were noted in air voids (Figure 4), along the aggregate-paste interfaces, in the cement paste matrix, and to a lesser extent along micro-cracks. The circumstances surrounding these occurrences were consistent with sulfate attack. Due to the drainage conditions associated with the track relative to the surrounding terrain, there was a high degree of exposure to ground water however; limited testing of soil and water samples for sulfate indicated that the likelihood of the ground water being a source of sulfate was extremely low. This finding tended to preclude (to a large extent) the possibility of external sulfate attack being the cause of ettringite formation assuming that the sulfate content in soil and water remained the same for the past 10-15 years. It was evident however (due to the reason stated above), that the existing concrete had been subject to considerable exposure to ground water over the 14 year period.

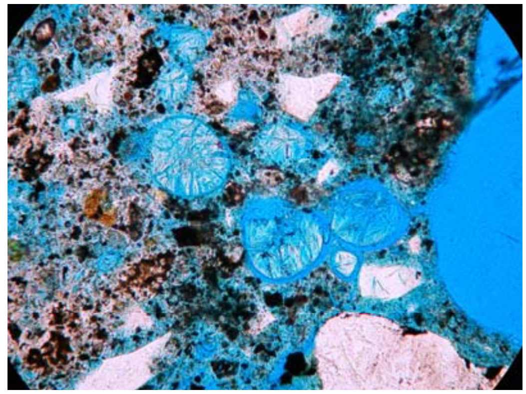

Figure 4 Ettringite in air voids.

2. Examples of evidence of alkali-silica reaction were found such as (i) crack passing through the aggregates (Figure 5a), (ii) presence of altered gel (Figure 5b) and in places (iii) presence of strained quartz (strained quartz is alkali-silica reactive) were observed, however conclusive evidences of ASR such as (i) presence of confirmed un-altered gel, (ii) severe aggregate cracking, (iii) reaction rim etc. were not observed. Alteration of calcium hydroxide and C-S-H due to carbonation was frequently observed at the aggregate-paste interfaces and also in the concrete matrix. It is suspected that carbonation may have altered the ASR

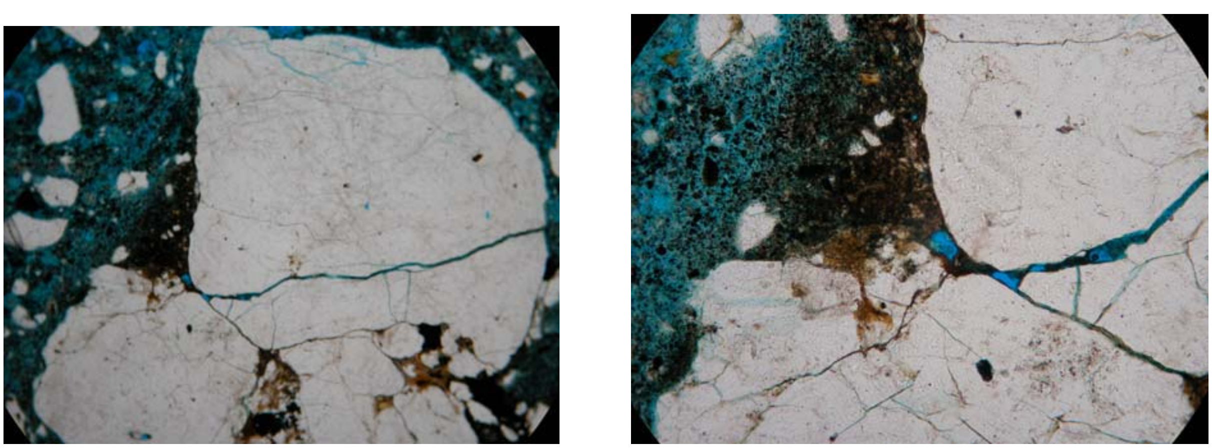

(a) (b) magnified view of (a)

Figure 5 Aggregate cracking and possibly altered ASR gel.

gel (Figure 5b) at least in some instances where the evidences of ASR and carbonation occur intimately. Further petrographic-related work on additional representative specimens would have been useful to facilitate (i) confirmation of the absence or presence of ASR, (ii) the frequency of ASR gel and (iii) chemical composition of ettringite and ASR gel using selective SEM-EDS.

Improvements Provided by Track Reconstruction

Due to expansion and contraction over 14 years, the track at BMS developed a convex shape which forced single file racing. This in combination with the fact that the radial transitions between the steeply banked oval turns and the tangent sections were relatively short effectively eliminated a portion of the track to the racing field due to the tendency of the reverse slope to push fast moving traffic into the perimeter crash wall. Passing involved moving a racer in front out of the primary travel path by bumping them from behind which, although interesting from a fan's point of view, created a dangerous situation for the drivers and pit crewman. A parabolic or concave transverse profile was needed that would allow the cars to keep speed and position at any groove or position on the track.

Early in the design process, the concave transverse profile of the track was to be limited only to the radius sections. However, constructability and overall driver safety concerns dedicated the extension of the concave profile through the tangent section as well. To this end, Eberly and Associates, Atlanta, Georgia, designed the transverse geometrics based on a profile change of 6 inches from the transverse center of the track to the edge effectively allowing a car on the outer portion of the track to travel at a faster pace than a car on the inner portion of the track. With this capability, the vehicles on the outer portions of the track (while taking advantage of inertia forces to hold the car to the track as it moves from the turns to the tangent sections) keep pace with a vehicles on the inner portions of the track even though they traveled through a greater distance. The transitions were designed such that a car coming out of a turn is constantly subject to inertia forces allowing the racer to enter the turns at high speeds under a great downward force. This also eliminated the need to race in a single file while accommodating passing lanes on any part of the track. This approach, which has been in the dirt track racing industry for several years, was validated (Figure 6) during a recent racing event. With 3 wide racing over 2500 passes for position changes took place where previously at BMS only 900 passes occurred in 500 laps of single file racing.

Figure 6 Racing 3 wide August 25, 2007.

Pavement Design and Joint Movement

A continuously reinforced concrete (CRC) pavement was the selected pavement type for the BMS track reconstruction. Given the load conditions associated with the use of the track a design thickness of 7 inches would be more than adequate for performance purposes especially since a bonded 4 inch lean concrete base was incorporated in the pavement cross-section. Due to concerns of the stability of freshly placed concrete on the steep slopes through the track radii, the surface of the lean concrete base was given a roughened finish to ensure a mechanical bond to the concrete while it was in a fresh state. Consequently, a bonded condition between the base and the surface layer was assumed in the determinations of the composite pavement thickness and the design steel content for the track. The composite pavement thickness relative to the required steel content was determined using parallel composite theory (Young et al, 1998):

$$h_e = \frac{E_c}{E_c} h_c + \frac{E_b}{E_c} h_b = 7 + \frac{1.3}{4} 4 = 8.3 \text{ inches}$$

The above computation is based upon assumed modular layer values of the base (E_b = 1.3 x 10^6 psi) and the surface concrete (E_c= 4.0 x 10^6 psi) of 0.33). The method described by Zollinger (2007) was employed to estimate the average crack spacing, distribution, and width which were 54 and 0.031 inches, respectively based on a composite thickness of 8.3 inches and a steel percentage of 0.80%. Crack spacing prediction (L) was determined according to:

$$\bar{L} = \frac{\{f_t - f_\sigma\}}{\frac{f}{2} + \frac{U_m P}{c_1 d_b}}$$

where:

$\bar{L}$ = Mean crack spacing, (inch)
f_t = Tensile strength of the concrete, (psi)
f_σ = Maximum stress in concrete at steel level, (psi)
f = Friction coefficient
U_m = Peak bond stress, (psi)
P = Percent of longitudinal reinforcement, percent
d_b = Reinforcing steel bar diameter, (in)
c_1 = Bond-slip coefficient

and crack width (cw) according to:

$$cw_i = \bar{L}\left(\varepsilon_{shr} + \alpha_{PCC}\Delta T\right) - \bar{L}\frac{c_2}{E_{PCC}}\left(\frac{\bar{L}\, U_m P_b}{c_{1i} d_b} + C\sigma_0\left(1 - \frac{2h_s}{h_{PCC}}\right) + \frac{\bar{L}}{2} f\right)$$

where:

$\bar{L}$ = Crack spacing, in
ε_{shr} = Unrestrained concrete drying shrinkage at the steel depth
α_{PCC} = Concrete CTE, °C^{-1} (°F^{-1})
ΔT = Drop in PCC temperature at the depth of the steel for time increment i (°F)
c_1 = First bond stress coefficient
c_2 = Second Bond stress coefficient

E_{PCC} = Concrete modulus of elasticity, (psi)
P_b = Percent of longitudinal reinforcement expressed as a fraction
d_b = Reinforcing steel bar diameter, (in)
U_m = Peak bond stress, (psi)
h_{PCC} = PCC slab thickness, (in)
h_s = Depth to steel, (in)
f = Subbase friction coefficient from test data or using AASHTO recommendations.
C = Bradbury's correction factor for slab size
$\square_0$ = Westergaard nominal environmental stress factor, (psi)

Figure 7 illustrates the expected crack pattern distribution for the BMS CRC resulting from the design steel content and expected temperature drop which was conservatively selected from available climate data for the Bristol region as 100°F.

Finite Element Analysis

The objective of the finite element analysis was to determine the contraction-induced displacement (due to thermal and drying shrinkage strains) at the four construction joint locations of the track previously noted. This type of analysis was used because the inner (and outer) edges of the circular portion of the track were to be restrained radially by a double wall lug system (discussed later), but unrestrained tangentially (Figure 8). The construction joints were to be positioned at the junction of the circular and straight portion of the track.

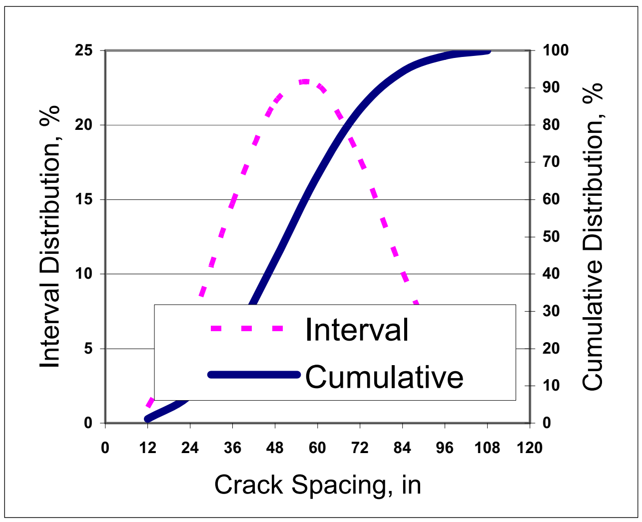

Figure 7 Predicted Crack Space Distribution.

The finite element analysis was formulated using 2D plane stress elements. Rigid body restraint was applied on either side of the track to simulate the presence of the retaining and lug walls. The track was then subjected to a 100°F contractive temperature and allowed to decrease volumetrically. The displacements were computed throughout the track length.

The analysis was conducted for a variety of frictional restraint conditions. One case, the concrete slab was considered to rest on a frictionless subgrade. This approach would overestimate displacement due to the contractive strain.

Another case was formulated to indirectly accommodate the effect of friction between the slab and underlying support. For a 2D plane stress or plane strain element, it is not

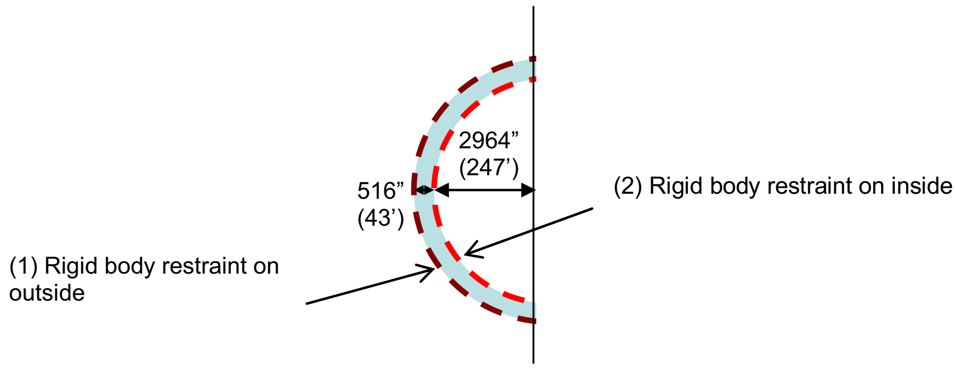

Figure 8 Geometry considered for FEM analysis.

possible to directly introduce friction beneath the pavement during analysis. However, tangential friction values can be assigned between the rigid body constraints on either side of the track and the edge of the track, i.e. at the contact interfaces (1) and (2) as shown in Figure 8. Therefore, the friction resistance experienced by the concrete section due to the subgrade was accommodated by introducing a coefficient of friction between the track and the rigid body restraints on either side to represent the same level of restraint afforded by the subbase friction.

Tangential friction between the track and the rigid body restraint was mobilized by applying a normal force. In the case of friction between the pavement and subgrade the normal force is mobilized due to the weight of the slab which is about 300 lb per running inch of the track. Therefore, in order to mobilize the friction on the two edges of the track, radial outward pressure acting on both edges with magnitude of 150 psi was applied (for plane stress the section thickness is set to 1”). Translating the frictional restraint between the base and slab to the edges and slab and applying a normal force required to mobilize equivalent magnitude of frictional restraint, it was possible to obtain a more realistic estimate for the displacement due to the contractive strain. It should be noted that the resulting tangential stresses in the concrete slab were not considered for the design. However, the effect of friction tangentially from the results as noted below appeared to be useful.

For the case without friction, a radial inward contraction of about 0.13″ and a longitudinal contraction of about 2″ at each transverse joint were determined from the analysis (Figure 9 – in the x direction). Radial stresses along the inner edge of the track were estimated to determine the reaction force on the lug wall due to the contractive strains. This reaction force varied from approximately + 25 psi (tensile on lug wall which will be largely offset by the self weight component due to inclination of the track) to - 9 psi (compressive on lug wall). These stresses are in addition to approximately 20 psi (acting on 7″ thickness of the wall) due to the self weight component. The self weight component arising due to the track inclination, especially in the circular portion of the track was found to be the most critical for design.

The estimate of displacement (Figure 10) in this circumstance most likely overestimates behavior under field conditions. For the subsequent analysis, the effect of friction was incorporated in the form of friction between the track and the rigid body restraint on either side, as previously noted. In this case, the displacement in the transverse joint was determined to be approximately 1.5” for a 100°F drop in temperature when the coefficient of friction was 1.0. Figure 10a illustrates the comparison of displacement along the circular portion of the track with and without friction. A similar analysis was conducted for the straight portion of the track (Figure 10b). Table 1 summarizes the results for the displacement from these calculations but it is noted that a friction coefficient of 1.5 along the edge was needed to approximate a friction coefficient of 1.0 along the subbase.

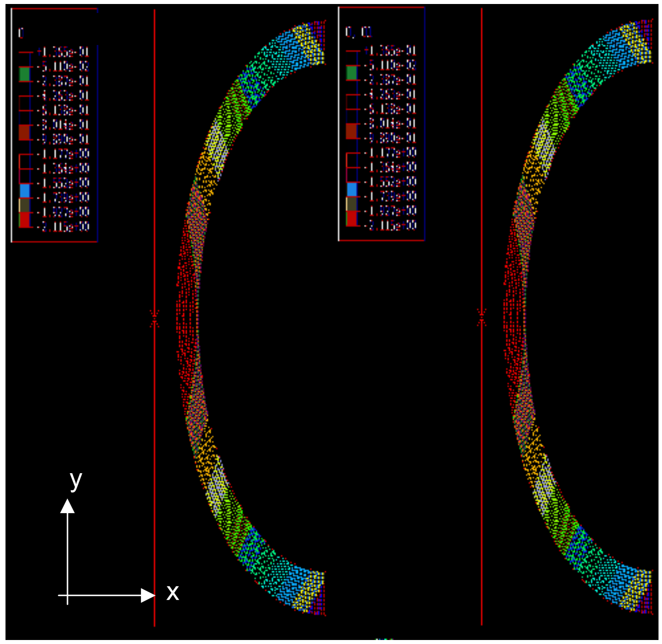

Figure 9 Displacement in the circular part of track.

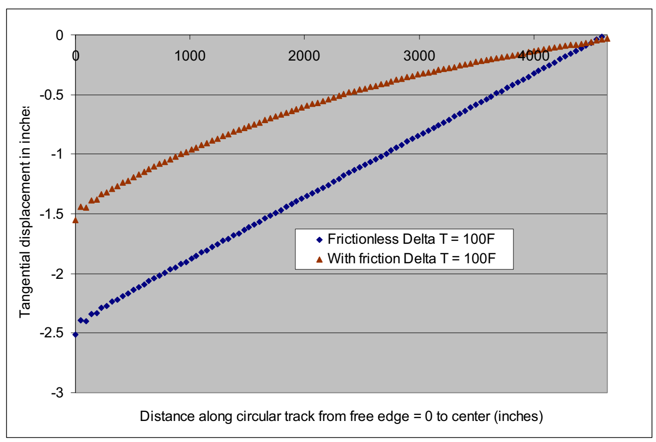

Figure 10a Contraction the circular portion.

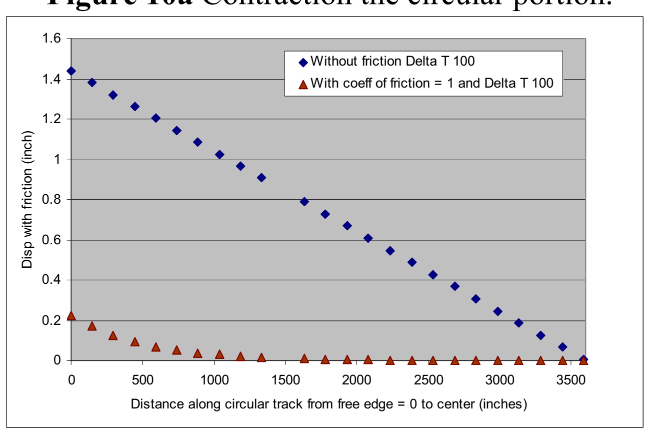

Figure 10b Contraction in the straight portion.

<u>Lateral Steel Distribution and Crack Control</u>

Solutions of stress analysis of thick-walled cylinders, which is analogous to the stress patterns in the CRC pavement through the radius sections of the track indicate a greater level of tangential stress (σ_t) to the interior of the track boundaries. To this end, a special case of the theoretical solution by Lamé (Seely and Smith, 1952) is useful to understand the change in stress level from the inner to outer track boundaries (ρ):

$$\sigma_t = p_1 \frac{r_1^2}{r_2^2 - r_1^2}\left(\frac{r_2^2}{\rho^2} + 1\right)$$

where

p_1 = Pressure along the inner track boundary
r_1 = Inner radius of the track boundary
r_2 = Outer radius to the track boundary

Table 1 Summary of Displacements due to Contraction Strain.

Coefficient of Friction (along edge of track)	**Displacement for 100°F Drop Induced Strain**		
	Circular Portion	**Straight Portion**	**Total**
0	2.60”	1.40”	4.00”
1.0	1.50”	0.20”	1.70”
1.5	1.00”	0.12”	1.12”

According to this expression, σ_t varied from $6.28p_1$ at the inner boundary to $5.28p_1$ at the outer boundary which is an 84% change across the transverse cross-section of the track. The bar spacing (bspc) for 0.8% longitudinal steel, found from the following expression:

$$\text{bspc} = \frac{\pi * d_b^2}{4(\%p)h_e} = \frac{\pi * \left(\frac{5}{8}\right)^2}{4(0.008)8.3} = 4.6 \text{ in.}$$

could also be used to determine the lateral distribution of the steel (Figure 11) by varying the steel content by 8% to either boundary to adjust the steel content according to Lamé’s solution. Accordingly, the steel percentage at the inner boundary would be 0.86% (bspc = 4.3 inches) and the steel percentage at the outer boundary would be 0.74% (bspc = 5.0 inches).

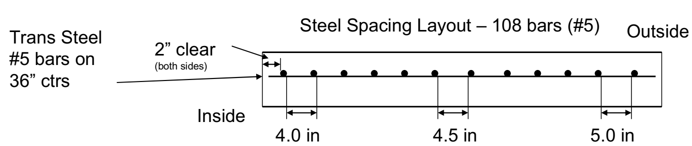

Figure 11 Lateral Steel Distributions.

It is noted that an internal pressure situation exists as it would occur for the contractive conditions described above relative to restraint of the track due the anchoring of the banked sections. Accordingly, the inside of the track was anchored by a double wall lug system to minimize movement of the track to the interior of the race track (Figure 12). As was noted previously, the movement of the previous track section in this regard was aggravated by the restraint of the expansion joints that were also located at the quarter points of the track oval. The details of this analysis are not provided here other than to note that the 150 lbs/in internal pressure determined from the finite element analysis (for a friction factor of 1.5 along the edge) was used to determine the depth of the restraint lugs to prevent over turning.

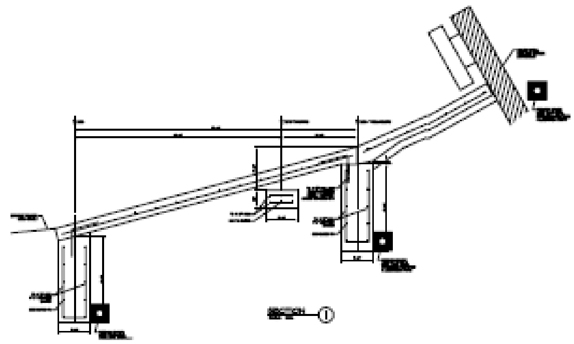

Figure 12 Anchor Lug System.

As also previously noted, an interesting aspect of the track design (Figure 13) and construction was the lack of a bond breaker in the track cross-section due to a concern for stability of the fresh concrete during the placement stages. The roughened finish of the lean concrete base helped to mitigate this condition but also increased the probability of cracking reflecting into the CRC pavement at an early age which could have performance consequences since cracks such as these may widen uncontrollably over the life of the pavement. Figure 13 illustrates the recommended notching pattern to minimize the propensity for wide cracks to form. Early sawcut notches placed in the lean concrete base at 10 foot intervals were covered with a bond breaking material to minimize reflection cracking tendencies of the base layer. The sawcut notches in the surface concrete were located at 5 intervals (as the predicted crack spacing was 54 inches) to initiate cracks at the surface and promote top down cracking. Placement of the steel at a depth of 3 inches would also help promote this type of cracking.

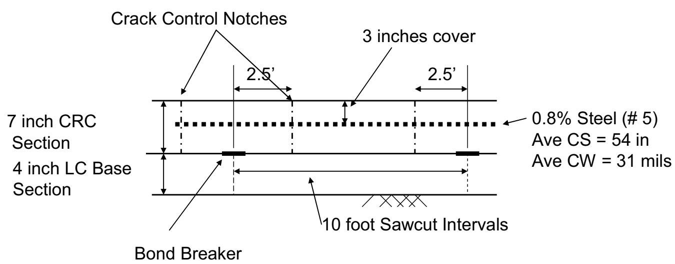

Figure 13 Location of Sawcuts to Induce Cracking.

Performance

Recent surveys of the cracking pattern in the newly constructed CRC pavement at the BMS have indicated that random cracking was largely controlled by the early notching. As part of the survey, crack and joint measuring points were established to monitor selected crack and joint movements in the pavement. Sawcut notches were placed during construction on 5 foot intervals (see Figure 14a and b) to insure crack initiation from the pavement surface. The notching operation was specially engineered for this project for these close intervals however the 5 foot interval was only maintained on the straight away portions of the track where the notch interval was 10 feet through the radius portions. The results of the crack survey are summarized in Appendix A in Table A.1; the data indicates that nearly all of the random transverse cracking occurred in the radius areas.

There was noted debonding along the expansion joints where the joint sealant had separated from the inside wall of the joint (Figure 15). The width of these joints was approximately 1 inch in October 2007 and 1.5 inch in January 2008 where the temperature was approximately 15°F. The concrete set temperature was approximated to be 100°F which means the temperature drop was approximately 85°F. It appears that construction preparation may have played a role in the debonding since the joint was originally placed at approximately 0.75 inches. The net opening is approximately 0.75 inches at a temperature change of 85°F compared to a predicted opening of 1.12 inches (from Table 1) at a temperature drop of 100°F which is an over estimate of approximately 22% (this of coarse assumes the contribution due to drying shrinkage is incorporated in the temperature drop).

Figure 14a Sawing in the Banked Sections (Gomaco World, 2008)

Figure 14b 5 Foot Sawcuts.

Observations to date indicate crack widths to be uniformly distributed and average less than 20 mils (with a range from 15 to 30 mils but one crack in the radius was 35 mils wide). However, in the radiuses, some cracks varied in width (of about 10 mils) from the inside to the outside of the track for a distance of 24 to 30 inches from the inside edge signifying that the highest stress level is in that portion of the track. Instances where the sawcuts are apparently closely aligned with a transverse crack (as noted in Table A.1) most likely failed to properly initial cracking. Approximately 8 and 15% of the sawcuts in the North and South ends of the track, respectively, were closely aligned with random transverse cracks. Due to the grouping of some of this type of cracking, timing of the sawcut may have played a role in the capability of the notch to control the random cracking. However, since more than half of the random cracks occurred in the center of the sawcut segments, it seems likely that those cracks would have been controlled with the sawcutting at a 5 foot interval rather than a 10 foot interval. Nonetheless, the sawcutting operations were for the most part very successful and all of the transverse

Figure 15 Expansion Joint.

cracking is well distributed and is expected to contribute to the long term performance of the track pavement. Even at a 10 foot interval, the sawcutting appeared to be very effective as evidenced by the observed uniformity of the crack widths.

The crack survey also noted 4 longitudinal cracks in the pavement; two were on the West side and two were on the East side of the track in the tangent areas. These cracks are relatively short and should be of little consequence.

Conclusions

The design and construction of a CRC pavement for the BMS oval configuration provided the following unique challenges:

- Design of transverse profile through the turns on to the straight sections
- Design and prediction of the expansion joint openings to accommodate the unique displacement conditions represented by the oval configuration.
- Accommodate the non-uniform transverse distribution of tensile stress
- Design elements to maintain the position of the banked portions of the track
- Design aspects for crack initiation to prevent wide reflection cracks from forming in the pavement

The design of the transverse parabolic concave profile appears to be very successful and made a significant difference in how the races at BMS are run. The design methodology for crack spacing prediction for CRC pavement incorporated in the new AASHSTO Guide is robust and appeared to work well in conjunction with the early surface notching methodology used in this project to minimize the effects of early random crack development. Although, construction limitations may have played a role in the timing and spacing application of the notches, the effectiveness of the methodology is very good. The early sawing also seemed to promote the uniformity of the transverse crack widths particularly through the radius sections. The double wall lug system seemed to be performing well as evidenced by the wider cracks along the inner track edge. However limiting the finite method was to representing the frictional constraints of the track, the estimated joint movement was reasonable as far as design purposes but certainly the analytical technique could be improved. The causes of the durability cracking of the existing concrete were not definitively determined but it seems that the reactivity of the coarse aggregate due to ASR may have played a role.

It is noted this project was awarded the prestigious Harold J. Halm Presidential Award from the American Concrete Pavement Association.

Acknowledgements

The authors are grateful for the support of the Bristol Motor Speedway in the development of the design details for the reconstructed track and the Continuous Steel Reinforcing Institute (CSRI) in supporting the collection of the performance data.

References

Zollinger, Dan G. “The Mechanistic Approach behind the Design for CRC Pavement Cracking in the 200x AASHTO Guide,” International Conference on Concrete Roads Johannesburg, South Africa, August 16-17 2007.

J. Francis Young, Sidney Mindess, Robert J. Gray, and Arnon Bentur, “The Science and Technology of Civil Engineering Materials,” Prentice Hall, Inc., New Jersey, 1998.

Seely, Fred B. and James O. Smith, “Advanced Mechanics of Materials,” Second Edition, John Wiley & Sons, Inc., New York, 1952.

Gomaco World, vol. 36, No. 1, Ida, Iowa, 2008.

Appendix A
Survey Data

Table A.1 Random Cracking Details (as of 23 Oct 07).

Station Location	Type	Length	Remarks
2 + 50	Transverse	6 inches	
3 + 35		Full width	Near 10’ sawcut
3 + 40		Full width	
4 + 60		4 feet	
5 + 05		15 feet	Near 10’ sawcut
5 + 40		4 feet	
6 + 05		15 feet	Near 10’ sawcut
6 + 25		12 feet	Near 10’ sawcut
6 + 40		16 feet	
6 + 55		16 feet	Near 10’ sawcut
6 + 60		16 feet	
7 + 05		22 feet	Near 10’ sawcut
7 + 70		14 feet	
8 + 30		25 feet	
8 + 80		15 feet	
9 + 15		3 feet	Near 10’ sawcut
9 + 20		28 feet	
9 + 70		3 feet	
10 + 40		28 feet	
10 + 50		10 feet	
15 + 40		5 inches	In tangent section
15 + 55		20 feet	In tangent section Near 10’ sawcut
15 + 65		15 feet	Near 10’ sawcut
16 + 90		24 feet	
16 + 95		10 feet	Near 10’ sawcut
17 + 90		20 feet	
17 + 95		20 feet	Near 10’ sawcut
18 + 15		20 feet	Near 10’ sawcut
18 + 40		14 feet	
19 + 65		25 feet	Near 10’ sawcut
19 + 85		28 feet	Near 10’ sawcut
20 + 20		14 feet	
20 + 30		10 feet	
20 + 35		20 feet	Near 10’ sawcut
20 + 60		30 feet	
20 + 85		14 feet	Near 10’ sawcut
21 + 15		15 feet	Near 10’ sawcut
21 + 30		10 feet	

Station Location	**Type**	**Length**	**Remarks**
21 + 55		30 feet	Near 10’ sawcut
21 + 75		30 feet	Near 10’ sawcut
21 + 95		20 feet	Near 10’ sawcut
22 + 20		15 feet	
22 + 30		20 feet	
22 + 40		30 feet	
22 + 50		35 feet	
22 + 70		30 feet	
22 + 95		16 feet	Near 10’ sawcut